ACS APPLIED MATERIALS & INTERFACES

Research Article

www.acsami.org

Structure of Nitrogen and Zirconium Co-Doped Titania with Enhanced Visible-Light Photocatalytic Activity

Peng Zhang,[†,§] Yanlong Yu,[†] Enjun Wang,[‡] Jingsheng Wang,[†] Jianghong Yao,[†] and Yaan Cao*[,†]

[†]Key Laboratory of Weak-Light Nonlinear Photonics, Ministry of Education, TEDA Applied Physics Institute and School of Physics, Nankai University, Tianjin 300457, China

[‡]Hefei Institutes of Physical Science, Chinese Academy of Sciences, Hefei 230031, China

[§]China Electronics Technology Group Corporation 54th Research Institute, Shijiazhuang 050000, China

Supporting Information

ABSTRACT: Nitrogen and zirconium co-doped TiO_2 (TiO_2−N−x% Zr) photocatalysts were synthesized via a sol−gel method. The existing states of the dopants (N and Zr) and their corresponding band structures were investigated via XRD, Raman, BET, XPS, TEM, FT-IR, UV−vis DRS, and PL techniques. It was found that N existed only as a surface species (NO_x) and Zr^{4+} was doped in a substitutional mode; the doping of Zr^{4+} ions and modification of N extended the absorption into the visible region and inhibited the recombination of electrons and holes. Moreover, the excess Zr^{4+} ions existed as the $ZrTiO_4$ phase when the content of Zr was sufficiently high, which could also contribute to the separation of the charge carriers. Therefore, the TiO_2−N−x%Zr samples show enhanced visible-light photocatalytic activity compared with single-doped TiO_2. These results offer a paradigm for the design and fabrication of optoelectronic functional materials such as solar cells and photocatalysts.

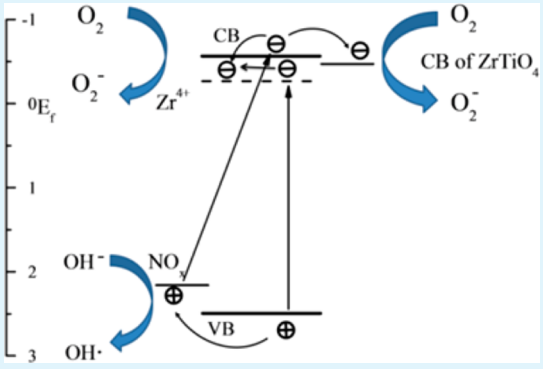

KEYWORDS: *TiO_2, surface NO_x species, substitutional Zr^{4+} ions, $ZrTiO_4$, visible-light photocatalysis, 4-chlorophenol degradation*

1. INTRODUCTION

Titanium dioxide (TiO_2) is considered to be one of the most attractive semiconductors to date and has been applied as a photocatalyst for the purification of pollutants.[1−4] However, limited by its large band gap (anatase, 3.2 eV),[5,6] TiO_2 shows no response to solar light, which impedes the effective usage of solar illumination in its practical applications. In spite of this, TiO_2 presents quite a low quantum yield as a result of its high recombination rate of photogenerated electrons and holes.[7,8]

Doping TiO_2 with foreign ions is a promising approach to extend its response to the visible-light region;[9−20] a breakthrough in this regard was made in 2001 via the doping of TiO_2 with nitrogen.[11] From that point forward, nitrogen-doped TiO_2 has been investigated widely by many other researchers owing to its great potential for enhancing visible-light activity.[15,21−25] As a titanium subgroup element, Zr possesses the same valence shell structure $(n-1)d^2ns^2$ and valence state as Ti. Accordingly, Zr^{4+}-doped TiO_2 has attracted the interest of many researchers because of its benefits for use in increasing the photocatalytic activity of TiO_2.[14,20,26−28]

Furthermore, doping TiO_2 with multiple dopants has become an effective and promising approach to improve the photocatalytic performance of TiO_2.[6,8,29−31] Our recent work has demonstrated that TiO_2 co-doped with (N, Sn)[6] or (N, In)[32] exhibits improved visible-light photocatalytic activity in comparison with nitrogen-doped TiO_2. In addition, TiO_2 doped with N and Zr has been investigated by some researchers. For example, Liu et al.[33] prepared nitrogen and zirconium co-doped TiO_2 nanotube arrays that exhibited improved photocatalytic efficiency. Gao et al.[34] synthesized nitrogen-doped $Ti_{1-x}Zr_xO_2$ that demonstrated an extended visible-light response. However, the existing states of the dopants for Zr and N co-doped TiO_2 and their corresponding band structures have still not been explored, and the influence of the dopants' existing states on the absorption and behavior of the photogenerated carriers as well as the photocatalytic mechanism of the photocatalysts still needs to be investigated further.

In this work, TiO_2 doped with nitrogen and zirconium catalysts were prepared via a sol−gel method. It was found that the modified N was present as a surface species (NO_x) and the introduced Zr^{4+} ions were weaved into the anatase lattice in a substitutional mode, whereas the excess Zr^{4+} ions formed $ZrTiO_4$ on the surface. The doped Zr^{4+} ions in the substitutional mode and the surface NO_x species both contributed to the remarkable absorption of these catalysts in

Received: April 29, 2013
Accepted: March 14, 2014
Published: March 14, 2014

the visible-light region. Moreover, these features as well as the $TiO_2/ZrTiO_4$ interface contributed to the separation of charge carriers. Accordingly, the photocatalytic activity of TiO_2−N−10%Zr was enhanced by upward of about three times that of TiO_2−N.

2. EXPERIMENTAL SECTION

2.1. Photocatalyst Preparation. Deionized water (>18.2 MΩ cm) was used in all experiments, and the chemicals used were of analytical grade. Zr and N co-doped photocatalysts were prepared by the following steps. First, a certain quantity of zirconium oxychloride ($ZrOCl_2$) was added into a mixture of 1 mL of water and 40 mL of anhydrous ethanol at room temperature. Under vigorous stirring, 12 mL of $Ti(OC_4H_9)_4$ and 1 mL of a concentrated HCl solution (12 M) was added into the solution dropwise. Three milliliters of ammonia was added, and a white precipitate was formed at once. After aging for 24 h at room temperature, the resultant precipitate was dried at 100 °C and then calcined at 450 °C for 12 h. The obtained photocatalysts were denoted TiO_2−N−x%Zr, where x% represented the nominal molar percentage of Zr^{4+} ions relative to the total abundance of Zr^{4+} and Ti^{4+} ions (Zr/(Zr + Ti)). TiO_2−N and TiO_2−x%Zr were synthesized using the same process but without the addition of $ZrOCl_2$ or ammonia, respectively. Pure TiO_2 was synthesized without any corresponding doping reagent.

2.2. Photocatalyst Characterization. A Rigaku D/Max-2500 X-ray diffraction spectrometer (Cu Kα, λ = 1.54056 Å) was used to acquire the XRD patterns. The BET surface area of the samples was determined via nitrogen adsorption−desorption isotherm measurement at 77 K (Micromeritics automatic surface area analyzer Gemini 2360, Shimadzu). XPS measurements were carried out with an ESCA Lab 220i-XL spectrometer with an unmonochromated Al Kα (1486.6 eV) X-ray source. All spectra were calibrated to the binding energy of the adventitious C 1s peak at 284.8 eV. The diffuse reflectance UV−vis absorption spectra were collected on an UV−vis spectrometer (U-4100, Hitachi). Fluorescence was generated by irradiating the samples at ambient temperature with an NT342/3/UVE laser source (a combination of a nanosecond Nd:YAG (NL303G, 325 nm) laser, harmonics generators (SHG, THG), and an optical parametric oscillator (OPO; PG122)), which was collected and focused into a spectrometer (MS3504) and detected using an optical signal detector (PMT, Hamamatsu R928). The system also included a data acquisition unit (DAQ), a digitizer (pico ADC-200/100), and optics for excitation beam guiding and luminescence signal collecting. Transmission electron microscopy (TEM) and high-resolution TEM (HRTEM) analysis were conducted using a JEM-2010FEF, for which the samples were prepared by applying a drop of an ethanol suspension onto an amorphous carbon-coated copper grid and drying naturally. Infrared transmission spectra were recorded for KBr disks containing the powder sample with an FTIR spectrometer (Bruker Tensor 27). Each spectrum was the result of adding 16 scans collected at a 4 cm^{-1} resolution.

2.3. Evaluation of Photocatalytic Performance. The photocatalytic performance of the as-prepared photocatalysts was evaluated by monitoring the degradation of 4-chlorophenol (4-CP) (40 mL, 5 × 10^{-5} M, pH 5.38) under visible-light irradiation (λ > 400 nm). The photocatalyst dosage was 10 mg, which was suspended in 4-CP solution. A sunlamp (Philips HPA 400/30S, Belgium) was used as the light source, and a 400 nm cutoff filter was employed to remove ultraviolet light. The reactor was placed perpendicular to the light beam and was located 10 cm away from the light source. The visible-light intensity on the photocatalysts' surface was 0.1 W cm^{-2}. The 4-CP solution was continuously bubbled with O_2 gas at a flux of 5 mL min^{-1} under stirring at 25 ± 2°C. The concentration of residual 4-CP was measured every 2 h using a UV-vis spectrometer (UV-1061PC, Shimadzu) with 4-aminoantipyrine as the chromogenic reagent. Prior to the photocatalytic reactions, the suspension was stirred in the dark for 30 min to reach adsorption equilibrium of 4-CP onto the photocatalysts. Each photocatalytic experiment was repeated three times, and the reproducibility of the results was found to be within acceptable deviation (±2%).

3. RESULTS AND DISCUSSION

3.1. Determination of Crystallite Structure. The XRD patterns of the TiO_2 (curve a), TiO_2−N (curve b), TiO_2−10% Zr (curve c), TiO_2−N−x%Zr (curves d−g), and TiO_2−40%Zr (curve h) samples are shown in Figure 1. It was found that

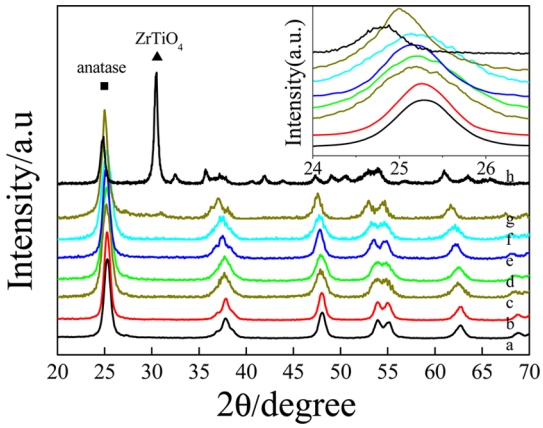

Figure 1. XRD patterns of TiO_2 (curve a), TiO_2−N (curve b), TiO_2−10%Zr (curve c), TiO_2−N−5%Zr (curve d), TiO_2−N−10%Zr (curve e), TiO_2−N−15%Zr (curve f), TiO_2−N−20%Zr (curve g), and TiO_2−40%Zr (curve h). The inset is the enlargement of the XRD peaks for the (101) plane.

anatase is the major crystal phase for all of the samples.[28] For the TiO_2−40%Zr sample, with the exception of the peaks of anatase, there were new diffraction peaks observed at 30.5, 32.9, and 42.1°, corresponding to the (111), (020), and (121) crystal planes of $ZrTiO_4$, respectively. This indicates that $ZrTiO_4$ formed in the TiO_2−40%Zr sample during the synthesis process. For TiO_2−N−20%Zr (curve g), a weak peak at about 30.5° was detected, which is ascribed to $ZrTiO_4$, suggesting the formation of a small amount of $ZrTiO_4$. In addition, no characteristic diffraction peak for other chemical species of nitrogen or zirconium (such as TiN and ZrO_2) was detected for all samples.

The enlargement of the XRD peaks for the (101) plane of all samples is plotted in the inset of Figure 1. No shift in the peak position was observed for TiO_2−N when compared with pure TiO_2, whereas the peaks of the TiO_2−10%Zr, TiO_2−40%Zr, and TiO_2−N−x%Zr samples shift to lower diffraction angle. The diffraction peaks of the (101) and (200) planes for all samples were used to evaluate the lattice parameters as well as the crystal size and are summarized in Table 1. Compared with TiO_2, the lattice parameters and cell volume of TiO_2−N are almost unchanged, whereas those of the TiO_2−10%Zr, TiO_2−40%Zr, and TiO_2−N− x%Zr samples increase. The doping mechanism will be discussed in detail in the following sections.

According to doping theory, doped ions can substitute for the lattice ions in the oxide if their ionic radii are close.[18] Because the ionic radius of Zr^{4+} ions (72pm) is slightly larger than that of Ti^{4+} ions (53 pm), an increase in the cell volume and lattice parameters is expected after Zr^{4+} ions replace the lattice Ti^{4+} ions and occupy their positions. In the case of nitrogen, there should be an appreciable change in the lattice parameters and cell volume if the nitrogen ions (171pm) substitute for the lattice oxygen ions (140pm). However, no

dx.doi.org/10.1021/am405510a | ACS Appl. Mater. Interfaces 2014, 6, 4622−4629

Table 1. Lattice Parameter, Crystal Size, and Specific Surface Area for TiO_2, TiO_2−N, TiO_2−10%Zr, and TiO_2−N−*x*%Zr

samples	lattice parameter (Å) $a = b$	lattice parameter (Å) c	cell volume (Å^3)	crystal size (nm)	specific surface area ($m^2\ g^{-1}$)
TiO_2	3.788	9.515	136.50	17.92	71.66
TiO_2−N	3.786	9.521	136.50	16.93	94.02
TiO_2−10%Zr	3.795	9.534	137.30	8.07	110.52
TiO_2−N−5%Zr	3.786	9.595	137.21	9.29	94.88
TiO_2−N−10%Zr	3.795	9.571	137.84	9.07	101.87
TiO_2−N−15%Zr	3.799	9.572	138.14	8.40	107.68
TiO_2−N−20%Zr	3.819	9.692	141.33	7.56	119.66

change was found for the lattice parameters and cell volume of TiO_2−N compared with TiO_2, indicating that doping nitrogen into TiO_2 in a substitutional mode can be excluded. Therefore, according to the XRD results, it is reasonable to speculate that Zr can incorporate into the TiO_2 matrix in a substitutional mode and N can exist as a surface species,[6] which will be further investigated in the following sections. In addition, the crystallite size of the TiO_2−N, TiO_2−10%Zr, and TiO_2−N−*x*%Zr samples decreased in comparison with pure TiO_2, indicating that the introduced nitrogen and/or zirconium can provide disparate boundaries and resulting in the inhibition of the growth of TiO_2 crystals. Moreover, it can be clearly seen that the specific surface areas agree well with the trend for the change in the crystal size for all samples.

Figure 2 shows the Raman patterns of the TiO_2, TiO_2−N, and TiO_2−N−*x*%Zr photocatalysts. For all samples, the

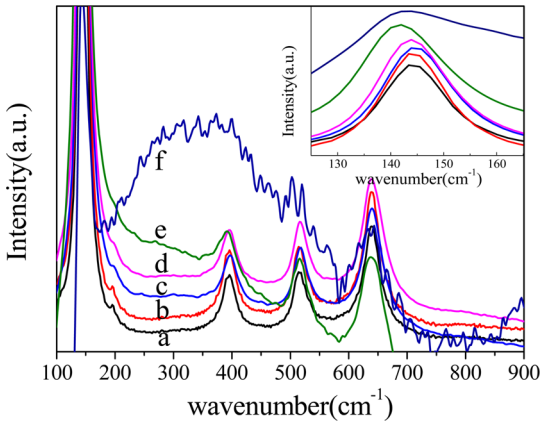

Figure 2. Raman patterns of TiO_2 (a), TiO_2−N (b), TiO_2−N−5%Zr (c), TiO_2−N−10%Zr (d), TiO_2−N−15%Zr (e), and TiO_2−N−20% Zr (f). An enlargement of the E_g vibrational modes for TiO_2 is shown in the inset.

vibration bands at 144, 197, 396, 516, and 640 cm^{-1} are ascribed to the E_g, B_{1g}, A_{1g}, B_{1g}, and E_g vibrational modes of titania, suggesting the existence of the anatase structure.[35] A vibration band at around 280 cm^{-1} can be observed for TiO_2−N−15%Zr (e) and TiO_2−N−20%Zr (f), corresponding to one of the vibrational modes of $ZrTiO_4$.[36] The peak of $ZrTiO_4$ can also be found in the Raman pattern of the TiO_2−15%Zr and TiO_2−20%Zr samples (Figure S1). Compared with pure TiO_2, the shift of the Raman E_g peak (144 cm^{-1}) of TiO_2−N was not observed, indicating that the doping of nitrogen into TiO_2 through the substitutional mode can thus be excluded. Moreover, the Raman E_g peak (144 cm^{-1}) of both the TiO_2−x%Zr (inset in Figure S1) and TiO_2−N−*x*%Zr (inset in Figure 2) samples shifts to lower wave numbers based on the increment of zirconium content, which implies that the doping Zr^{4+} ions exist in the TiO_2 lattice in a substitutional mode. After the lattice Ti^{4+} ions are replaced by Zr^{4+} ions, the Zr−O bond formed in the lattice. Because the ionic radius of lattice Ti^{4+} (53 pm) is smaller than that of Zr^{4+} (72 pm), the length of the Ti−O bond is shorter than that of the Zr−O bond. As a result, a tensile stress in the lattice is induced, leading to a decrease in the vibrational energy of the 144 cm^{-1} (E_g) band and corresponding to the O−Ti−O bond bending vibration.[35] Therefore, the peaks at 144 cm^{-1} (E_g) for the Zr^{4+}-doped TiO_2 samples shift to lower frequencies compared with that of pure TiO_2. The Raman results are in good agreement with the XRD results.

3.2. Determination of the Existence State of Nitrogen and Zirconium. XPS was used to study the existing states of the dopants and the N 1s spectra of the TiO_2−N−*x*%Zr samples (*x* = 5, 10, and 15) as well as TiO_2−N, and the data are plotted in Figure 3. A broad peak centered at about 399.8 eV

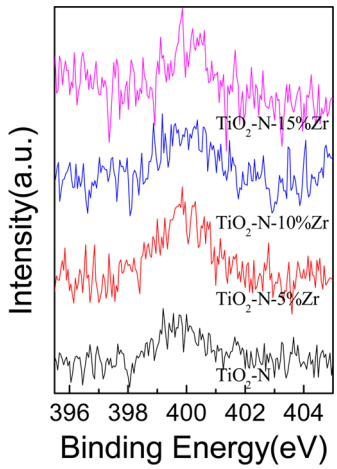

Figure 3. N 1s spectra for TiO_2−N−*x*%Zr (*x* = 5, 10, and 15) and TiO_2−N.

was observed for all of the samples, which is higher than the binding energy (BE) of 396.7 eV in TiN,[37] indicating that the nitrogen ions interact strongly with oxygen atoms.[24] Therefore, the BE at about 399.8 eV could be ascribed to NO_x species, suggesting the formation of a Ti−N−O linkage on the surface of the TiO_2−N and TiO_2−N−*x*%Zr samples.[38−41] The formation of NO_x species was also confirmed by the FTIR spectra (Figure S2).

The XPS Zr 3d spectra of TiO_2−N−*x*%Zr (*x* = 5, 10, and 15) are shown in Figure 4, and the atom percent of Zr and N derived from the XPS spectra is shown in Table 2. The peak located at around 182.0 eV is ascribed to the Zr $3d_{5/2}$ peak of the substitutionally introduced Zr^{4+} ions because the peak falls between the Zr $3d_{5/2}$ peaks of ZrO_2 (183.5 eV)[42] and metallic Zr (179.0 eV).[43] In addition, in comparison with TiO_2, the peaks of O 1s and Ti 2p shift to a higher BE for TiO_2−N−*x*% Zr (Figures S3 and S4) as the doped Zr^{4+} content increases. This indicates that more Zr^{4+} ions were incorporated into the TiO_2 lattice and replaced the lattice Ti^{4+} ions as the amount of doped Zr increased. Because the electronegativity of Ti (1.5) is smaller than that of Zr (1.6), it is possible that the electrons

dx.doi.org/10.1021/am405510a | ACS Appl. Mater. Interfaces 2014, 6, 4622−4629

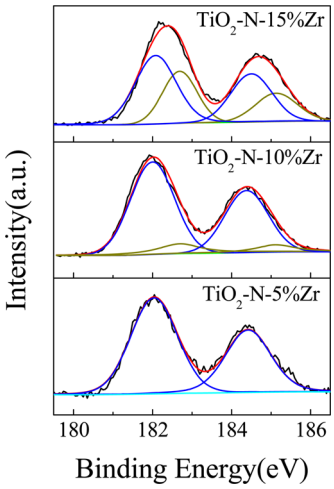

Figure 4. Zr 3d spectra of TiO_2−N−5%Zr, TiO_2−N−10%Zr, and TiO_2−N−15%Zr.

Table 2. Atom Percent (%) of Zr and N in Ti, O, Zr, and N Calculated from the XPS Spectra

	Zr 3d		N 1s
sample	Sub. Zr	$ZrTiO_4$	NO_x
TiO_2−N−5%Zr	2.62		0.79
TiO_2−N−10%Zr	4.97	0.76	0.70
TiO_2−N−15%Zr	5.74	3.42	0.76

would be induced to transfer from Ti^{4+} to Zr^{4+} in the Zr−O−Ti links. Such a charge transfer would increase the binding energy of the Ti 2p and O 1s core electrons.[19] Moreover, new double peaks centered at around 182.6 eV were found for the TiO_2−N−10%Zr and TiO2−N−15%Zr samples, which is ascribed to the Zr $3d_{5/2}$ peak of $ZrTiO_4$.[44]

HRTEM images of TiO_2 and TiO_2−N−20%Zr are shown in Figure 5. It is obvious that the fringe spacing of the (101)

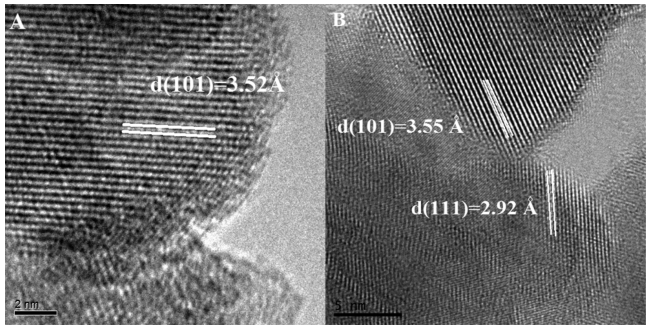

Figure 5. HRTEM image of pure TiO_2 (A) and TiO_2−N−20%Zr (B) samples.

crystallographic plane for pure TiO_2 and TiO_2−N−20%Zr is ca. 3.52 and 3.55 Å, respectively. In comparison with TiO_2, the increase in the fringe spacing for TiO_2−N−20%Zr confirms that Zr^{4+} ions were weaved into the TiO_2 lattice in a substitutional mode. In addition, a new fringe spacing of 2.92 Å was found on the surface of TiO_2 nanoparticles and is ascribed to the (111) plane of $ZrTiO_4$. Therefore, the HRTEM images confirm that the Zr^{4+} ions are weaved into the TiO_2 lattice in a substitutional mode, whereas the rest of the Zr^{4+} ions exist in $ZrTiO_4$, resulting in the formation of the TiO_2/$ZrTiO_4$ interface.

According to the aforementioned results, we conclude that the introduced nitrogen mainly exists as NO_x species and forms Ti−N−O linkages on the surface of TiO_2; for the introduced zirconium, when the content is low (x = 5), Zr^{4+} ions were doped only into TiO_2 lattice in substitutional mode; when the content is sufficiently high (x = 10, 15, and 20), besides the substitutional Zr^{4+} ions, $ZrTiO_4$ species are present on the surface of TiO_2−N−x%Zr, forming the TiO_2/$ZrTiO_4$ interface.

3.3. Band Structure and Visible-Light Response. Diffuse reflectance UV−vis absorption spectra and XPS valence band (VB) spectra were performed to investigate the band structure of the samples. Figure 6A shows the diffuse reflectance UV−vis absorption spectra for the TiO_2, $ZrTiO_4$, TiO_2−N, TiO_2−10%Zr, and TiO_2−N−x%Zr samples. The strong absorption at about 330 nm is caused by the band−band transition of TiO_2. The band gap is about 3.05 eV for pure TiO_2 because the band threshold is located at 406 nm. Similarly, the band gap for $ZrTiO_4$ was determined to be 3.24 eV because the threshold is located at 382 nm. The small hump at around 450 nm for TiO_2−N is a typical trait of N-modified TiO_2 and arises from the electron transition from the energy level of the NO_x species (0.3 eV above the VB of TiO_2) to the conduction band (CB) of TiO_2.[22,40] In addition, the absorption edge for TiO_2−N did not shift compared with pure TiO_2, indicating that the surface NO_x species do not change the band gap. Compared with pure TiO_2, the absorption edge of the TiO_2−10%Zr and TiO_2−N−x%Zr samples blueshift to 402 nm, which is caused by the quantum size effect and corresponds to a band gap of 3.08 eV. For the TiO_2−10%Zr sample, a strong absorption in the visible-light region was found and is ascribed to the electron transition from the VB to the energy level of substitutionally doped Zr^{4+} ions.[45] The inset of Figure 6 shows the difference DRS spectra acquired by subtracting the absorption spectra of TiO_2 from that of TiO_2−10%Zr. The absorption maximum was around 443 nm, corresponding to an energy gap of ca. 2.80 eV. Thus, the doping energy level of the substitutional Zr^{4+} ions was deduced to be 0.28 eV below the CB of TiO_2−10%Zr. Moreover, the TiO_2−N−x%Zr samples show enhanced absorption in comparison with TiO_2−N and TiO_2−10%Zr from 400 to 800 nm (Figure 6). This contribution comes from a synergistic effect of the surface NO_x species and substitutionally doped Zr^{4+} ions, suggesting that nitrogen and zirconium co-doped TiO_2 is more photosensitive to solar light than single-doped TiO_2.

In addition, XPS valence band spectra (Figure 6B) were used to locate the VB maximum of $ZrTiO_4$ and TiO_2. The work function (E_f, Fermi level) of the XPS instrument (4.10 eV vs vacuum level) is at 0.00 eV. It has been demonstrated both theoretically and experimentally that the upper VB shows strong hybridization (σ bonding) between the Ti 3d and O 2p orbitals and that the maximum of the VB is dominated by O 2p orbitals.[46,47] Hence, the binding energy of the onset edge of the O 2p peak reveals the energy gap between the maximum of the VB and Fermi level (E_f).[5] The VB maximum was determined to be 2.52 eV for TiO_2 and 2.78 eV for $ZrTiO_4$, and the difference of the VB maximum for $ZrTiO_4$ and TiO_2 is 0.26 eV. The CB minimum for TiO_2 and $ZrTiO_4$ is −0.56 and −0.46 eV, respectively, because the band gap is 3.08 eV for the TiO_2−N−x%Zr samples and 3.24 eV for $ZrTiO_4$. Therefore, the corresponding energy levels for the different materials and dopants are summarized in Table 3. The corresponding band

dx.doi.org/10.1021/am405510a | ACS Appl. Mater. Interfaces 2014, 6, 4622−4629

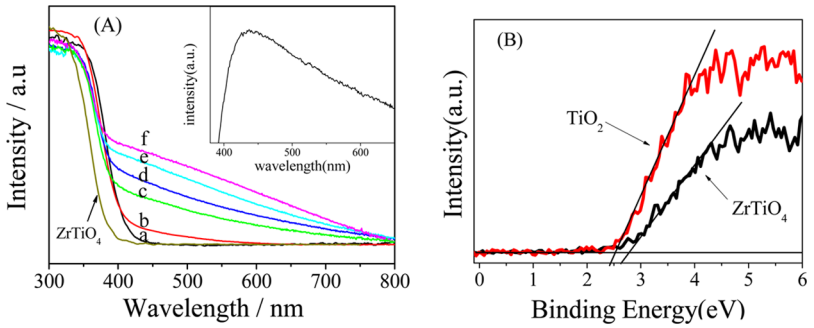

Figure 6. (A) Diffuse reflectance UV−vis absorption spectraof TiO_2 (a), TiO_2−N (b), TiO_2−10%Zr (c), TiO_2−N−5%Zr (d), TiO_2−N−10%Zr (e), and TiO_2−N−15%Zr (f). The inset shows the difference DRS spectra of TiO_2−10%Zr. (B) XPS valence band spectra of TiO_2 and $ZrTiO_4$.

Table 3. Position of the Energy Levels for Different Materials and Dopants

energy level	CB of TiO_2 (eV)	CB of $ZrTiO_4$ (eV)	doped Zr^{4+} ions (eV)	NO_x species (eV)	VB of TiO_2 (eV)
position	−0.56	−0.46	−0.28	2.22	2.52

structure for the the TiO_2−N−x%Zr samples is drawn and shown in Figure 10.

3.4. Photoluminescence Spectra. Figure 7 shows the photoluminescence (PL) spectra for all samples. There are two peaks observed for pure TiO_2 (centered at about 520 and 460 nm), which could be ascribed to the transition from the oxygen vacancy with one trapped electron and two trapped electrons, respectively.[48−50] Therefore, the energy levels for these vacancies were calculated to be about 0.48 and 0.79 eV below the CB.

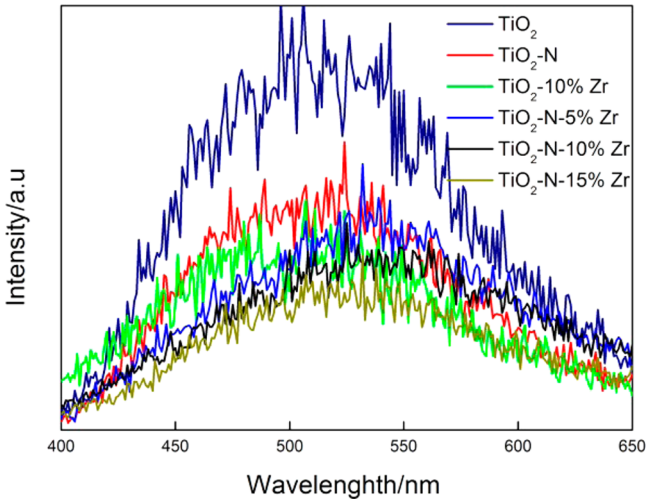

Figure 7. Photoluminescence spectra of all of the samples (TiO_2, TiO_2−N, TiO_2−10%Zr, and TiO_2−N−x%Zr).

A decrease in PL intensity indicates an inhibition of recombination of charge carriers. The modification of TiO_2 with nitrogen caused an effective quenching of the PL intensity because the surface energy level of the NO_x species acts as a hole trapper. The PL intensity of the TiO_2−10%Zr sample also decreased in comparison with TiO_2 because of the substitutionally doped Zr^{4+} ions. Because the energy level of substitutionally doped Zr^{4+} ions (0.28 eV below the CB) is higher than those of the oxygen vacancies (0.48 and 0.79 eV below the CB), the excited electrons in the CB would move to the doping energy level of the Zr^{4+} ions rather than to those of the oxygen vacancies, resulting in a decrease in the emission intensity. A further decrease of the PL intensity was observed after TiO_2 was co-doped with N and Zr because of the efficient capture of photogenerated carriers by the energy levels of both NO_x and Zr^{4+} ions. In addition, the PL intensity further decreased with an increase in the Zr content for the TiO_2−N−x%Zr samples because of the occurrence of the $TiO_2/ZrTiO_4$ interface (0.1 eV below the CB). Hence, the PL results indicate

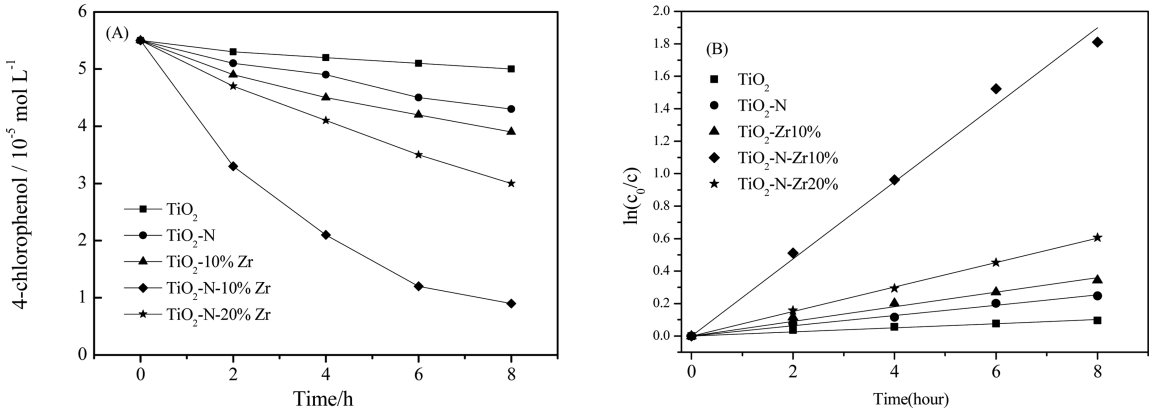

Figure 8. Photodegradation of 4-CP (A) and relationship of $\ln(c_0/c)$ to reaction time (B) for TiO_2, TiO_2−N, TiO_2−10%Zr, TiO_2−N−10%Zr, and TiO_2−N−20%Zr under visible-light irradiation.

dx.doi.org/10.1021/am405510a | ACS Appl. Mater. Interfaces 2014, 6, 4622−4629

that co-doping with nitrogen and zirconium as well as the $TiO_2/ZrTiO_4$ interface effectively separates the photogenerated charge carriers, implying the enhanced photocatalytic activity of this material.

3.5. Photocatalytic Activity. The photodegradation of 4-CP under visible-light irradiation ($\lambda \geq 400$ nm) was applied to evaluate the photocatalytic performance of all samples (Figures 8 and 9 and Table 4). The $\ln(c_0/c)$ values of 4-CP for all of the samples exhibit a linear relation with the time of the reaction (Figure 8B), suggesting that a pseudo-first-order reaction took place for the degradation of 4-CP. As shown in Figure 8A, 4-CP molecules are barely decomposed with pure TiO_2, whose photodegradation rate and specific photocatalytic activity of 4-CP are only 9.09% and 4.54×10^{-6} mol g^{-1} h^{-1}, respectively. TiO_2–N shows a higher photocatalytic activity than TiO_2 and has a photodegradation rate and specific photocatalytic activity of 4-CP of 21.82% and 1.09×10^{-5} mol g^{-1} h^{-1}, respectively. TiO_2–10%Zr presents an enhanced photocatalytic activity and has a photodegradation rate and specific photocatalytic activity of 4-CP of 29.10% and 1.46×10^{-5} mol g^{-1} h^{-1}, respectively. Among all samples, TiO_2–N–10%Zr exhibits the best photocatalytic activity, having a photodegradation rate (83.64%) and specific photocatalytic activity of 4-CP (4.18×10^{-5} mol g^{-1} h^{-1}) that is about four times that of TiO_2–N.

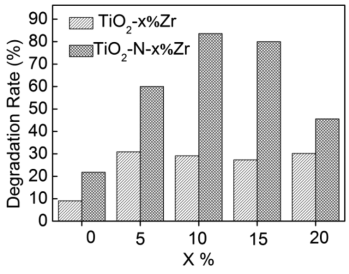

Figure 9. 4-CP degradation rates for TiO_2–x%Zr and TiO_2–N–x% Zr.

Figure 9 shows the degradation rates of 4-CP for the TiO_2–x%Zr and TiO_2–N–x%Zr samples. It is clear that the TiO_2–N–x%Zr samples exhibit higher degradation rates of 4-CP than the TiO_2–x%Zr samples when they share the same x values, suggesting that nitrogen and zirconium co-doping is an efficient method to improve the photocatalytic activity of a TiO_2-based catalyst. Moreover, TiO_2–N–10%Zr presented the best photocatalytic performance among the TiO_2–N–x%Zr samples. The photocatalytic performance decreased when the content of doped Zr^{4+} ions increased above 10% (such as TiO_2–N–15%Zr and TiO_2–N–20%Zr). This implies that the catalytic activity of TiO_2–N–x%Zr can be further enhanced by regulating the amount of nitrogen and zirconium simultaneously. The detailed photocatalytic mechanism will be discussed in the following section.

3.6. Photocatalytic Mechanism. According to the aforementioned results, the significantly enhanced photocatalytic activity for the photodegradation of 4-CP by the TiO_2–N–x%Zr samples could be explained by the schematic diagram of the band structure shown in Figure 10. The electrons can be excited directly from the VB of TiO_2 to the doping energy level of Zr^{4+} ions or from the surface energy level of NO_x species to CB of TiO_2 under visible-light irradiation (λ > 400 nm). Meanwhile, the photogenerated electrons in the CB of TiO_2 migrate to the energy level of the doped Zr^{4+} ions or transfer to the CB of $ZrTiO_4$ by crossing the $TiO_2/ZrTiO_4$ interface when the Zr content is sufficiently high (x > 10); the photogenerated holes in the VB move to the energy levels of the surface NO_x species. It turns out that the photogenerated charge carriers are separated efficiently. During the photocatalytic process, the 4-CP molecules adsorbed on the surface of TiO_2–N–x%Zr can be oxidized directly by holes in the energy level of the NO_x species or VB. Moreover, the photogenerated electrons in the doping energy level of the Zr^{4+} ions and the CB of $ZrTiO_4$ can be captured by the adsorbed O_2 on the surface of TiO_2–N–x%Zr, leading to the formation of O_2^- active species that degrade the 4-CP molecules further.[1,13]

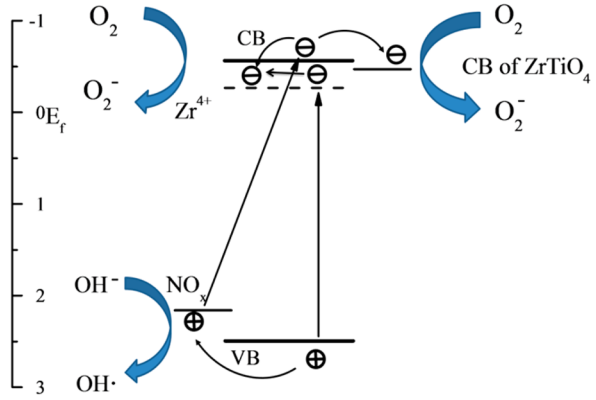

Figure 10. Band structure of TiO_2–N–x%Zr samples as well as their photocatalytic mechanism.

Under visible-light irradiation, pure TiO_2 can barely be excited as a result of its large band gap (3.05 eV), leading to a poor photocatalytic activity. For the TiO_2–N sample, only a small amount of electrons can be excited from the surface energy level of the NO_x species, resulting in a weak absorption around 450 nm and a limited photocatalytic performance. For the TiO_2–10%Zr samples, although the absorption becomes stronger in the visible-light region, the photocatalytic activity is still limited because of the relatively poor separation efficiency of electrons and holes. Compared with single-doped TiO_2, TiO_2 co-doped with nitrogen and zirconium shows enhanced absorption in the visible-light region and an increased amount of charge carriers. Furthermore, the energy level of substitu-

Table 4. Photodegradation of 4-Chlorophenol under Visible-Light Irradiation ($\lambda \geq 400$ nm)

sample	4-CP degraded $(c_0 - c)/c_0$ (%)[a]	k ($\times 10^{-4}$ h^{-1})[b]	$t_{1/2}$ (h)	specific photocatalytic activity (mol g^{-1} h^{-1})
TiO_2	9.09	119.1	59.9	4.54×10^{-6}
TiO_2–N	21.82	307.7	22.3	1.09×10^{-5}
TiO_2–10%Zr	29.10	406.4	16.7	1.46×10^{-5}
TiO_2–N–10%Zr	83.64	2262.6	2.8	4.18×10^{-5}

[a]After reaction for 8 h under visible-light irradiation. [b]Apparent rate constant deduced from the linear fitting of $\ln(c_0/c)$ versus the reaction time.

dx.doi.org/10.1021/am405510a | ACS Appl. Mater. Interfaces 2014, 6, 4622–4629

tionally doped Zr^{4+} ions and NO_x species as well as the CB of $ZrTiO_4$ in the TiO_2−N−10%Zr sample could separate the photogenerated electrons and holes effectively. Therefore, this leads to its better photocatalytic performance than TiO_2−10% Zr and TiO_2−N. Additionally, the increased specific surface area of the catalysts (Table 4) also contributes to the enhanced photocatalytic activity.

Nevertheless, the photocatalytic activity of the TiO_2−N−x% Zr samples decreases when the Zr content becomes greater than 10%. This may be caused by the increased defects on the $TiO_2/ZrTiO_4$ interface. Because the defects on the interface increase with the increase of $ZrTiO_4$, more photogenerated electrons in the CB of TiO_2 might recombine with holes through the defect energy level of $TiO_2/ZrTiO_4$, which would damage the photocatalytic process.

4. CONCLUSIONS

A new type of TiO_2-based visible-light photocatalyst (TiO_2−N−x%Zr) was synthesized by co-doping TiO_2 with nitrogen and zirconium via a sol−gel method. The introduced nitrogen exists only as a surface NO_x species. The Zr^{4+} ions were mainly doped into the TiO_2 lattice in a substitutional mode; additionally, the excess Zr^{4+} ions formed $ZrTiO_4$ species when the Zr content is sufficiently high. The coexistence of surface NO_x species and doped Zr^{4+} ions in a substitutional mode extended the absorption into the visible-light region and increased the total amount of charge carriers. Furthermore, the dopants and $TiO_2/ZrTiO_4$ interface separated the photogenerated electrons and holes efficiently. These results imply that doping TiO_2 with two metal and nonmetal ions is a more effective way to enhance the photocatalytic performance than doping with only one element. It is expected that detailed studies of the co-doped TiO_2 catalyst, especially to obtain more precise control over the alignment of the energy levels, will afford a viable approach to developing TiO_2-based photocatalysts that are better suited for practical applications.

■ ASSOCIATED CONTENT

Supporting Information

Raman patterns of TiO_2−x%Zr samples, FTIR spectra of TiO_2−N−x%Zr samples, and XPS Ti 2p and O 1s spectra of TiO_2−N and TiO_2−N−x%Zr samples. This material is available free of charge via the Internet at http://pubs.acs.org.

■ AUTHOR INFORMATION

Corresponding Author

*Fax: +86-22-66229310. Tel: +86-22-66229598. E-mail: caoya@nankai.edu.cn.

Notes

The authors declare no competing financial interest.

■ ACKNOWLEDGMENTS

This work was supported by the National Natural Science Foundation of China (nos. 51072082, 51372120, 51302269, and 21173121).

■ REFERENCES

(1) Hoffmann, M. R.; Martin, S. T.; Choi, W.; Bahnemann, D. W. Environmental Applications of Semiconductor Photocatalysis. *Chem. Rev.* **1995**, *95*, 69−96.

(2) Fujishima, A.; Zhang, X.; Tryk, D. TiO_2 Photocatalysis and Related Surface Phenomena. *Surf. Sci. Rep.* **2008**, *63*, 515−582.

(3) Chen, X.; Mao, S. S. Titanium Dioxide Nanomaterials: Synthesis, Properties, Modifications, and Applications. *Chem. Rev.* **2007**, *107*, 2891−2959.

(4) Tsai, C.-C.; Teng, H. Structural Features of Nanotubes Synthesized from NaOH Treatment on TiO_2 with Different Post-Treatments. *Chem. Mater.* **2006**, *18*, 367−373.

(5) Cao, Y.; He, T.; Chen, Y.; Cao, Y. Fabrication of Rutile TiO_2−Sn/Anatase TiO_2−N Heterostructure and Its Application in Visible-Light Photocatalysis. *J. Phys. Chem. C* **2010**, *114*, 3627−3633.

(6) Wang, E.; He, T.; Zhao, L.; Chen, Y.; Cao, Y. Improved Visible Light Photocatalytic Activity of Titania Doped with Tin and Nitrogen. *J. Mater. Chem.* **2010**, *21*, 144−150.

(7) Yuan, J.; Wu, Q.; Zhang, P.; Yao, J.; He, T.; Cao, Y. Synthesis of Indium Borate and Its Application in Photodegradation of 4-Chlorophenol. *Environ. Sci. Technol.* **2012**, *46*, 2330−2336.

(8) Wang, E.; Zhang, P.; Chen, Y.; Liu, Z.; He, T.; Cao, Y. Improved Visible-light Photocatalytic Activity of Titania Activated by Nitrogen and Indium Modification. *J. Mater. Chem.* **2012**, *22*, 14443−14449.

(9) Bowker, M.; James, D.; Stone, P.; Bennett, R.; Perkins, N.; Millard, L.; Greaves, J.; Dickinson, A. Catalysis at the Metal-Support Interface: Exemplified by the Photocatalytic Reforming of Methanol on Pd/TiO_2. *J. Catal.* **2003**, *217*, 427−433.

(10) Mukri, B. D.; Dutta, G.; Waghmare, U. V.; Hegde, M. S. Activation of Lattice Oxygen of TiO_2 by Pd^{2+} Ion: Correlation of Low-Temperature CO and Hydrocarbon Oxidation with Structure of $Ti_{1-x}Pd_xO_{2-x}$ (x = 0.01−0.03). *Chem. Mater.* **2012**, *24*, 4491−4502.

(11) Asahi, R.; Morikawa, T.; Ohwaki, T.; Aoki, K.; Taga, Y. Visible-light Photocatalysis in Nitrogen-Doped Titanium Oxides. *Science* **2001**, *293*, 269−71.

(12) Khan, S. U.; Al-Shahry, M.; Ingler, W. B. Efficient Photochemical Water Splitting by a Chemically Modified n-TiO_2. *Science* **2002**, *297*, 2243−2245.

(13) Cao, Y.; Yang, W.; Zhang, W.; Liu, G.; Yue, P. Improved Photocatalytic Activity of Sn^{4+} doped TiO_2 Nanoparticulate Films Prepared by Plasma-Enhanced Chemical Vapor Deposition. *New J. Chem.* **2004**, *28*, 218−222.

(14) Nagaveni, K.; Hegde, M.; Madras, G. Structure and Photocatalytic Activity of $Ti_{1-x}M_xO_{2\pm\delta}$ (M = W, V, Ce, Zr, Fe, and Cu) Synthesized by Solution Combustion Method. *J. Phys. Chem. B* **2004**, *108*, 20204−20212.

(15) Sakthivel, S.; Janczarek, M.; Kisch, H. Visible Light Activity and Photoelectrochemical Properties of Nitrogen-Doped TiO_2. *J. Phys. Chem. B* **2004**, *108*, 19384−19387.

(16) Zhu, J.; Zheng, W.; He, B.; Zhang, J.; Anpo, M. Characterization of Fe−TiO_2 Photocatalysts Synthesized by Hydrothermal Method and Their Photocatalytic Reactivity for Photodegradation of XRG Dye Diluted in Water. *J. Mol. Catal. A: Chem.* **2004**, *216*, 35−43.

(17) Debeila, M.; Coville, N.; Scurrell, M.; Hearne, G. The Effect of Calcination Temperature on the Adsorption of Nitric Oxide on Au-TiO_2: Drifts Studies. *Appl. Catal., A* **2005**, *291*, 98−115.

(18) Cao, Y.; He, T.; Zhao, L.; Wang, E.; Yang, W.; Cao, Y. Structure and Phase Transition Behavior of Sn^{4+}-doped TiO_2 Nanoparticles. *J. Phys. Chem. C* **2009**, *113*, 18121−18124.

(19) Wang, E.; Yang, W.; Cao, Y. Unique Surface Chemical Species on Indium Doped TiO_2 and Their Effect on the Visible Light Photocatalytic Activity. *J. Phys. Chem. C* **2009**, *113*, 20912−20917.

(20) Hernández-Alonso, M. D.; Coronado, J. M.; Bachiller-Baeza, B.; Fernández-García, M.; Soria, J. Influence of Structural and Surface Characteristics of Ti_{1-x} Zr_xO_2 Nanoparticles on the Photocatalytic Degradation of Methylcyclohexane in the Gas Phase. *Chem. Mater.* **2007**, *19*, 4283−4291.

(21) Sakthivel, S.; Kisch, H. Photocatalytic and Photoelectrochemical Properties of Nitrogen-Doped Titanium Dioxide. *ChemPhysChem* **2003**, *4*, 487−90.

(22) Lindgren, T.; Mwabora, J. M.; Avendaño, E.; Jonsson, J.; Hoel, A.; Granqvist, C.-G.; Lindquist, S.-E. Photoelectrochemical and Optical Properties of Nitrogen Doped Titanium Dioxide Films Prepared by Reactive DC Magnetron Sputtering. *J. Phys. Chem. B* **2003**, *107*, 5709−5716.

(23) Wu, P. G.; Ma, C. H.; Shang, J. K. Effects of Nitrogen Doping on Optical Properties of TiO_2 Thin Films. *Appl. Phys. A* **2004**, *81*, 1411−1417.
(24) Sathish, M.; Viswanathan, B.; Viswanath, R.; Gopinath, C. S. Synthesis, Characterization, Electronic Structure, and Photocatalytic Activity of Nitrogen-Doped TiO_2 Nanocatalyst. *Chem. Mater.* **2005**, *17*, 6349−6353.
(25) Gao, B.; Ma, Y.; Cao, Y.; Yang, W.; Yao, J. Great Enhancement of Photocatalytic Activity of Nitrogen-Doped Titania by Coupling with Tungsten Oxide. *J. Phys. Chem. B* **2006**, *110*, 14391−14397.
(26) Yu, J. C.; Lin, J.; Kwok, R. W. $Ti_{1-x}Zr_xO_2$ Solid Solutions for the Photocatalytic Degradation of Acetone in Air. *J. Phys. Chem. B* **1998**, *102*, 5094−5098.
(27) Chang, S.-m.; Doong, R.-a. Characterization of Zr-Doped TiO_2 Nanocrystals Prepared by a Nonhydrolytic Sol-Gel Method at High Temperatures. *J. Phys. Chem. B* **2006**, *110*, 20808−20814.
(28) Venkatachalam, N.; Palanichamy, M.; Arabindoo, B.; Murugesan, V. Enhanced Photocatalytic Degradation of 4-Chlorophenol by Zr^{4+} Doped Nano TiO_2. *J. Mol. Catal. A: Chem.* **2007**, *266*, 158−165.
(29) Zhao, W.; Ma, W.; Chen, C.; Zhao, J.; Shuai, Z. Efficient Degradation of Toxic Organic Pollutants with $Ni_2O_3/TiO_{2-x}B_x$ Under Visible Irradiation. *J. Am. Chem. Soc.* **2004**, *126*, 4782−4783.
(30) Cao, Y.; Yu, Y.; Zhang, P.; Zhang, L.; He, T.; Cao, Y. An Enhanced Visible-light Photocatalytic Activity of TiO_2 by Nitrogen and Nickel-Chlorine Modification. *Sep. Purif. Technol.* **2013**, *104*, 256−262.
(31) Yu, Y.; Wang, E.; Yuan, J.; Cao, Y. Enhanced Photocatalytic Activity of Titania with Unique Surface Indium and Boron Species. *Appl. Surf. Sci.* **2013**, *273*, 638−644.
(32) Wang, E.; Zhang, P.; Chen, Y.; Liu, Z.; He, T.; Cao, Y. Improved Visible-Light Photocatalytic Activity of Titania Activated by Nitrogen and Indium Modification. *J. Mater. Chem.* **2012**, *22*, 14443−14449.
(33) Liu, H.; Liu, G.; Shi, X. N/Zr-codoped TiO_2 Nanotube Arrays: Fabrication, Characterization, and Enhanced Photocatalytic Activity. *Colloids Surf., A* **2010**, *363*, 35−40.
(34) Gao, B.; Luo, X.; Fu, H.; Lin, B.; Chen, Y.; Gu, Z. Visible-Light-Driven Photocatalytic Performance of Nitrogen-Doped $Ti_{1-x}Zr_xO_2$ Solid Solution. *Mater. Res. Bull.* **2012**, *48*, 587−594.
(35) Zhang, W.; He, Y.; Zhang, M.; Yin, Z.; Chen, Q. Raman Scattering Study on Anatase TiO_2 Nanocrystals. *J. Phys. D: Appl. Phys.* **2000**, *33*, 912.
(36) Macan, J.; Gajović, A.; Ivanković, H. Porous Zirconium Titanate Ceramics Synthesized by Sol-Gel Process. *J. Eur. Ceram. Soc.* **2009**, *29*, 691−696.
(37) Saha, N. C.; Tompkins, H. G. Titanium Nitride Oxidation Chemistry: An X-ray Photoelectron Spectroscopy Study. *J. Appl. Phys.* **1992**, *72*, 3072−3079.
(38) Gopinath, C. S. Comment on "Photoelectron Spectroscopic Investigation of Nitrogen-Doped Titania Nanoparticles". *J. Phys. Chem. B* **2006**, *110*, 7079−7080.
(39) Sato, S.; Nakamura, R.; Abe, S. Visible-Light Sensitization of TiO_2 Photocatalysts by Wet-Method N Doping. *Appl. Catal., A* **2005**, *284*, 131−137.
(40) Sun, H.; Bai, Y.; Jin, W.; Xu, N. Visible-Light-Driven TiO_2 Catalysts Doped with Low-Concentration Nitrogen Species. *Sol. Energy Mater. Sol. Cells* **2008**, *92*, 76−83.
(41) Chen, X.; Lou, Y. B.; Samia, A. C.; Burda, C.; Gole, J. L. Formation of Oxynitride as the Photocatalytic Enhancing Site in Nitrogen-Doped Titania Nanocatalysts: Comparison to a Commercial Nanopowder. *Adv. Funct. Mater.* **2005**, *15*, 41−49.
(42) Bastl, Z.; Senkevich, A.; Spirovova, I.; Vrtilkova, V. Angle-Resolved Core-Level Spectroscopy of Zr1Nb Alloy Oxidation by Oxygen, Water and Hydrogen Peroxide. *Surf. Interface Anal.* **2002**, *34*, 477−480.
(43) Takano, I.; Isobe, S.; Sasaki, T.; Baba, Y. Nitrogenation of Various Transition Metals by N^+_2-Ion Implantation. *Appl. Surf. Sci.* **1989**, *37*, 25−32.
(44) Pandolfi, L.; Kaciulis, S.; Padeletti, G.; Cusma, A.; Viticoli, M. Deposition and Characterization of $ZrTiO_4$ Thin Films. *Surf. Interface Anal.* **2004**, *36*, 1159−1162.
(45) Wang, J.; Yu, Y.; Li, S.; Guo, L.; Wang, E.; Cao, Y. Doping Behavior of Zr^{4+} Ions in Zr^{4+}-Doped TiO_2 Nanoparticles. *J. Phys. Chem. C* **2013**, *117*, 27120−27126.
(46) Fleming, L.; Fulton, C.; Lucovsky, G.; Rowe, J.; Ulrich, M.; Luning, J. Local Bonding Analysis of the Valence and Conduction Band Features of TiO_2. *J. Appl. Phys.* **2007**, *102*, 033707-1−033707-7.
(47) Lin, Z.; Orlov, A.; Lambert, R. M.; Payne, M. C. New Insights into the Origin of Visible Light Photocatalytic Activity of Nitrogen-Doped and Oxygen-Deficient Anatase TiO_2. *J. Phys. Chem. B* **2005**, *109*, 20948−20952.
(48) Serpone, N.; Lawless, D.; Khairutdinov, R.; Pelizzetti, E. Subnanosecond Relaxation Dynamics in TiO_2 Colloidal Sols (particle sizes Rp = 1.0−13.4 nm). Relevance to Heterogeneous Photocatalysis. *J. Phys. Chem.* **1995**, *99*, 16655−16661.
(49) Yu, J. C.; Ho, W.; Yu, J.; Hark, S.; Iu, K. Effects of Trifluoroacetic Acid Modification on the Surface Microstructures and Photocatalytic Activity of Mesoporous TiO_2 Thin Films. *Langmuir* **2003**, *19*, 3889−3896.
(50) Saraf, L.; Patil, S.; Ogale, S.; Sainkar, S.; Kshirsager, S. Synthesis of Nanophase TiO_2 by Ion Beam Sputtering and Cold Condensation Technique. *Int. J. Mod. Phys. B* **1998**, *12*, 2635−2647.